2. Camps, M., Nichols, A. & Arkinstall, S. Dual specificity phosphatases: a gene family for control of MAP kinase function. *FASEB J.* **14,** 6–16 (2000).
3. Theodosiou, A. & Ashworth, A. MAP kinase phosphatases. *Genome Biol.* **3,** 3009–3018 (2002).
4. Martin-Blanco, E. *et al.* puckered encodes a phosphatase that mediates a feedback loop regulating JNK activity during dorsal closure in *Drosophila*. *Genes Dev.* **12,** 557–570 (1998).
5. Theodosiou, A., Smith, A., Gillieron, C., Arkinstall, S. & Ashworth, A. MKP5, a new member of the MAP kinase phosphatase family, which selectively dephosphorylates stress-activated kinases. *Oncogene* **18,** 6981–6988 (1999).
6. Tanoue, T., Moriguchi, T. & Nishida, E. Molecular cloning and characterization of a novel dual specificity phosphatase, MKP-5. *J. Biol. Chem.* **274,** 19949–19956 (1999).
7. Rincon, M., Derijard, B., Chow, C. W., Davis, R. J. & Flavell, R. A. Reprogramming the signalling requirement for AP-1 (activator protein-1) activation during differentiation of precursor $CD4^+$ T-cells into effector Th1 and Th2 cells. *Genes Funct.* **1,** 51–68 (1997).
8. Rincon, M. *et al.* Interferon-γ expression by Th1 effector T cells mediated by the p38 MAP kinase signaling pathway. *EMBO J.* **17,** 2817–2829 (1998).
9. Dong, C. *et al.* Defective T cell differentiation in the absence of Jnk1. *Science* **282,** 2092–2095 (1998).
10. Dong, C. *et al.* JNK is required for effector T-cell function but not for T-cell activation. *Nature* **405,** 91–94 (2000).
11. Janeway, C. A. Jr & Medzhitov, R. Innate immune recognition. *Annu. Rev. Immunol.* **20,** 197–216 (2002).
12. Takeuchi, O. *et al.* Differential roles of TLR2 and TLR4 in recognition of gram-negative and gram-positive bacterial cell wall components. *Immunity* **11,** 443–451 (1999).
13. Alexopoulou, L., Holt, A. C., Medzhitov, R. & Flavell, R. A. Recognition of double-stranded RNA and activation of NF-κB by Toll-like receptor 3. *Nature* **413,** 732–738 (2001).

Supplementary Information accompanies the paper on **www.nature.com/nature**.

Acknowledgements We thank L. Evangelisti, C. Hughes and J. Stein for technical assistance; P. Leder for providing TC-1 ES cells; R. Alanis for his help with the *Listeria* infection experiment; A. Farr for his guidance in animal studies; and the entire Dong laboratory for their support and help. R.J.D. and R.A.F. are HHMI investigators, and C.D. is an Arthritis Investigator of the Arthritis Foundation.

Competing interests statement The authors declare that they have no competing financial interests.

Correspondence and requests for materials should be addressed to R.A.F (richard.flavell@yale.edu) or C.D. (cdong@mdanderson.org).

Rb inactivation promotes genomic instability by uncoupling cell cycle progression from mitotic control

Eva Hernando[1]*, Zaher Nahlé[3]*†, Gloria Juan[1], Elena Diaz-Rodriguez[2], Miguel Alaminos[1]†, Michael Hemann[3], Loren Michel[2], Vivek Mittal[3], William Gerald[1], Robert Benezra[2], Scott W. Lowe[3] & Carlos Cordon-Cardo[1]

[1]*Department of Pathology and* [2]*Cancer Biology and Genetics Program, Memorial Sloan-Kettering Cancer Center New York, New York 10021, USA*
[3]*Cold Spring Harbor Laboratory 1 Bungtown Road, Cold Spring Harbor, New York 11724, USA*

* These authors contributed equally to this work.
† Present addresses: Department of Internal Medicine, Washington University in St. Louis, Saint Louis, Missouri, Missouri 63110, USA (Z.N.); Department of Histology, School of Medicine, University of Granada, Avenida de Madrid, 11. E-18012 Granada, Spain (M.A.)

Advanced human cancers are invariably aneuploid, in that they harbour cells with abnormal chromosome numbers[1,2]. However, the molecular defects underlying this trait, and whether they are a cause or a consequence of the malignant phenotype, are not clear. Mutations that disable the retinoblastoma (Rb) pathway are also common in human cancers[1]. These mutations promote tumour development by deregulating the E2F family of transcription factors leading to uncontrolled cell cycle progression[3]. We show that the mitotic checkpoint protein Mad2 is a direct E2F target and, as a consequence, is aberrantly expressed in cells with Rb pathway defects. Concordantly, Mad2 is overexpressed in several tumour types, where it correlates with high E2F activity and poor patient prognosis. Generation of Rb pathway lesions in normal and transformed cells produces aberrant Mad2 expression and mitotic defects leading to aneuploidy, such that elevated Mad2 contributes directly to these defects. These results demonstrate how chromosome instability can arise as a by-product of defects in cell cycle control that compromise the accuracy of mitosis, and suggest a new model to explain the frequent appearance of aneuploidy in human cancer.

The appearance of aneuploidy in human cancers has been linked to defects in several processes[1,2]. Many studies suggest that aneuploidy arises from defects in the conserved spindle checkpoint that normally governs progression through mitosis[4,5]. In response to lack of tension or improper microtubule attachment at the kinetochores, a group of sensor proteins (Bub3, Bub1, BubR1, Mps1 and Mad2) releases a diffusible signal that inhibits the ubiquitin ligase activity of the anaphase promoting complex (APC) or cyclosome[6]. APC/cyclosome function is required for sister chromatid separation and cytokinesis[7]. Although mitotic checkpoint defects are often observed in cancer cells challenged with microtubule poisons, and inactivation of checkpoint components produces aneuploidy in yeast and mammalian cells[8–10], loss-of-function mutations in spindle checkpoint genes are rarely observed in human tumours[11,12].

Adenovirus E1A is a potent viral oncoprotein that acts, in part, by inactivating the Rb gene product and deregulating the E2F transcription factors[3]. In performing a series of microarray experiments, we observed that E1A significantly increased the expression of *MAD2* (Z.N., V.M. and S.W.L., unpublished observations), a crucial component of the spindle checkpoint that associates with the APC/cyclosome, and prevents its activation[7,13]. Northern and western blot analyses of *MAD2* transcript and protein confirmed its upregulation by E1A in mouse embryo fibroblasts (MEFs) (Fig. 1a, compare lanes 1 and 2 or 3 and 4, respectively). Similarly, MEFs isolated from $Rb^{-/-}$ mice displayed increased Mad2 levels compared to $Rb^{+/+}$ controls (Fig. 1a, compare lanes 5 and 6). IMR90 human fibroblasts expressing either *E1A* (Fig. 1b, compare lanes 1 and 2) or *E2F-1* (Fig. 1b, compare lanes 1 and 3) also expressed elevated Mad2 levels, implying that deregulation of the Rb/E2F pathway induces Mad2 through a conserved mechanism.

The above results are consistent with the possibility that *MAD2* is an E2F target. Concordantly, previous global chromatin immunoprecipitation/microarray studies suggested that E2Fs can bind the *MAD2* promoter in normal fibroblasts[14]. Indeed, analysis of the *MAD2* genomic sequence showed several putative E2F-binding sites in the *MAD2* promoter (see Supplementary Fig. S1), and subsequent chromatin immunoprecipitation (ChIP) analysis confirmed *in vivo* binding of E2F-1 to their predicted sites in *E1A*-expressing cells (Fig. 1c, lane 2). Moreover, a *MAD2* genomic fragment containing the E2F sites (Supplementary Fig. S1) conferred E2F responsiveness to a luciferase reporter following transient transfection into IMR90 (data not shown) or U-2OS cells (Fig. 1d) in a manner comparable to the *caspase-7* promoter, an established E2F target[15]. Therefore, *MAD2* is a physiological transcriptional target of E2F.

Many E2F targets are cell-cycle regulated[3]. Therefore, we examined the cell cycle distribution of Mad2 expression in normal synchronously and asynchronously cycling cells. The level of Mad2 was undetectable in quiescent IMR90 cells (Fig. 1e, $t = 0$) and increased after cells entered S phase following serum addition, reaching maximum levels in G2/M, albeit slightly after cyclin A. The increase in Mad2 was confined largely to mitosis, as assessed by co-expression with phosphorylated histone H3 following release from a double-thymidine-induced S-phase arrest (Fig. 1f), and by laser scanning cytometry (LSC) analysis of Mad2 expression in unsynchronized NIH-3T3 fibroblasts (Fig. 1g). Presumably, Mad2 expression is regulated during the normal cell cycle as part of a

mechanism that coordinates the expression of spindle checkpoint proteins with the onset of G2/M.

E2F target genes are often constitutively expressed in cells with Rb pathway defects. Concordantly, Mad2 was expressed at aberrantly high levels throughout the cell cycle in IMR90 cells expressing E1A (Fig. 2a), which deregulates endogenous E2F, and in cells where *Rb* was suppressed by stable RNA interference (RNAi) (shRb[16], Fig. 2a). Of note, Mad2 levels in *E1A*- and *shRb*-expressing IMR90 cells were similar to those produced by enforced expression of *MAD2* (Fig. 2b, c). As in normal fibroblasts, Mad2 was confined to G2/M in the Rb-functional T24 bladder carcinoma[17] and HCT116 colon carcinoma lines (Fig. 2d). However, in bladder and colon carcinoma lines with inactive Rb, such as HT1197 (ref. 17) and SW480 (ref. 18), respectively, Mad2 was expressed at high levels throughout the cell cycle (Fig. 2d). Thus, cells with Rb defects often aberrantly express Mad2.

Because the Rb pathway is frequently disrupted during tumorigenesis, we asked whether Mad2 is overexpressed in human tumour specimens. Retinoblastomas, which invariably lose Rb function and deregulate E2F, expressed high levels of Mad2 relative to normal retina (Fig. 3a, upper panels). Similarly, Mad2 was significantly increased in many bladder carcinomas when compared to normal urothelium (data not shown), particularly in the more advanced tumours, where Rb inactivation is common[19] (Fig. 3a, middle panels). The elevated Mad2 levels observed in human tumours were not merely due to the increased proliferation of cancer cells, as Mad2 was not always detected in highly proliferating normal and tumour samples (see Supplementary Fig. S2).

A clear link between deregulated E2F activity and aberrant Mad2 expression was observed in neuroblastoma. Here, *MAD2* messenger RNA levels correlated tightly with *E2F1* mRNA expression (an E2F member but also a prototypical E2F target gene), as shown by analysis of a microarray database containing information on 106 neuroblastoma tumours and 12 neuroblastoma cell lines[20] (Fig. 3b; Kendall *tau* correlation coefficient: 0.568; $P < 0.0001$) and validated by immunohistochemistry (Fig. 3a, lower panels). Moreover, aberrant Mad2 expression was associated with *MYCN* (a proto-oncogene of the myelocytomatosis (*MYC*)-box genes) overexpression and amplification (which can drive E2F constitutive activation[21]) and poor patient prognosis (Fig. 3c). In fact, high Mad2 expression was more tightly associated with survival than *MYCN* amplification ($P = 0.001$ for *MAD2*; $P = 0.0215$ for *MYCN*). Interestingly, *MAD2* also clusters with tens of genes capable of predicting disease outcome in breast cancer patients[22]. Therefore, aberrant Mad2 expression is linked to Rb pathway defects in human tumours, where it can be an effective indicator of patient prognosis.

Most advanced human cancers are aneuploid, and loss of Rb function has been associated with mitotic defects[23]. Hence, it is paradoxical that cells with defective Rb express higher levels of a protein that should facilitate proper checkpoint responses. We hypothesized that misexpressed or elevated Mad2 might compromise mitotic events, predisposing cells to genomic instability. Therefore, we examined the DNA content of IMR90 fibroblasts expressing E1A, shRb or Mad2, all of which expressed similarly high levels of Mad2 throughout the cell cycle (see Fig. 2). Biparametric LSC analysis comparing BrdU incorporation and DNA content demonstrated that *E1A*-, *shRB*- and *MAD2*-transduced IMR90 or

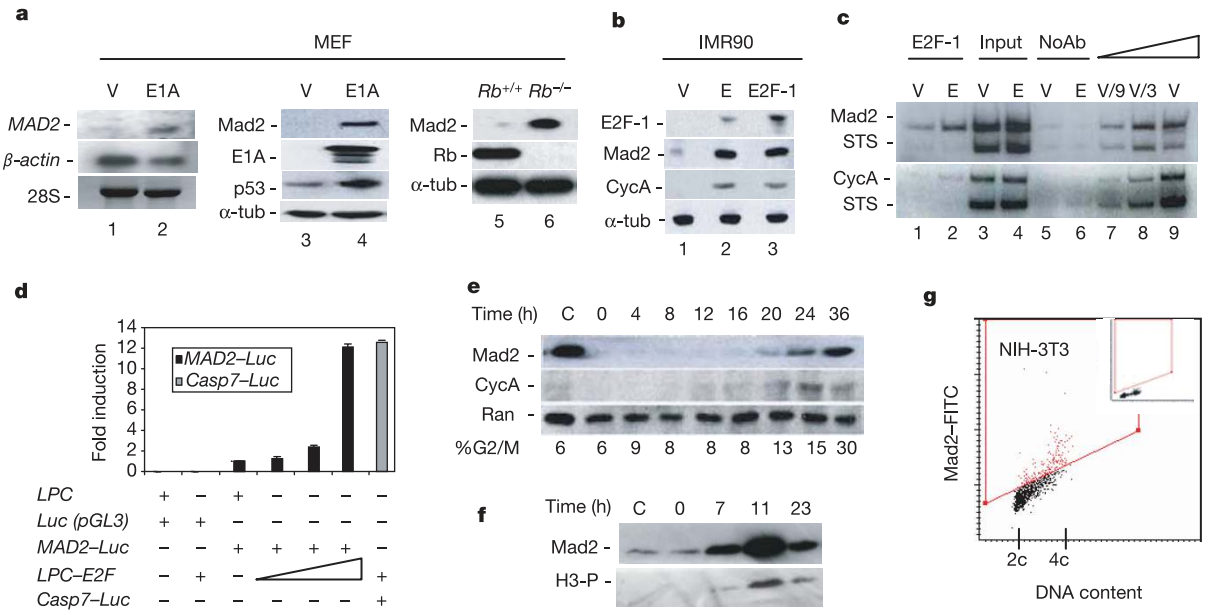

Figure 1 Mad2 is an E2F target. **a**, *MAD2* mRNA (lane 1 and 2) and protein (lane 3 and 4) were assessed in vector (V) or E1A-expressing MEFs by northern blotting and immunoblotting, respectively. p53 induction indicates E1A activity and α-tubulin (α-tub), β-actin or 28S RNA serve as loading controls. Mad2 protein levels were also compared in wild-type ($Rb^{+/+}$) and $Rb^{-/-}$ MEFs (lanes 5 and 6). **b**, Immunoblotting of the indicated proteins in IMR90 cells infected with vector- (V), *E1A*- (E) or *E2F-1*-expressing adenoviral constructs. Cyclin A (Cyc A) is an established E2F target. **c**, Chromatin immunoprecipitation[15] using an E2F-1 specific antibody in vector- (V) and E1A (E)-expressing IMR90 cells. Duplex PCR amplifications were performed using primers surrounding the putative E2F sites in the Mad2 promoter or the known sites in the cyclin A promoter, along with primers capable of amplifying Cyclin A genomic sequence (STS) lacking E2F binding sites (see Supplementary Fig. S1a). Input corresponds to PCR reactions containing 0.5% of total chromatin used in immunoprecipitation reactions. **d**, Relative luciferase signal in U-2OS cells co-transfected with empty vector (*LPC*) or *E2F-1* (*LPC–E2F*) and a luciferase reporter with (*MAD2–Luc*) or without (*Luc*) Mad2 promoter sequences. *E2F-1* plasmid concentration (triangle). The *Casp7–luc* reporter is the positive control. Values represent the mean ± s.e.m. ($n = 3$). **e**, Immunoblotting for Mad2 in control (C) or serum-starved IMR90 cells ($t = 0$), and at various times after serum addition. The percentages of cells in G2/M phase at the indicated time (shown below). **f**, Immunoblotting for Mad2 in IMR90 cells synchronized in S phase and released from a double-thymidine blockade. Histone H3-P is shown as a marker of mitosis. **g**, Mad2 expression by LSC in NIH-3T3 cells, where the gate represents the threshold considered positive for Mad2 based on the equivalent isotype control (inset). Cell populations of 2c and 4c DNA content are indicated.

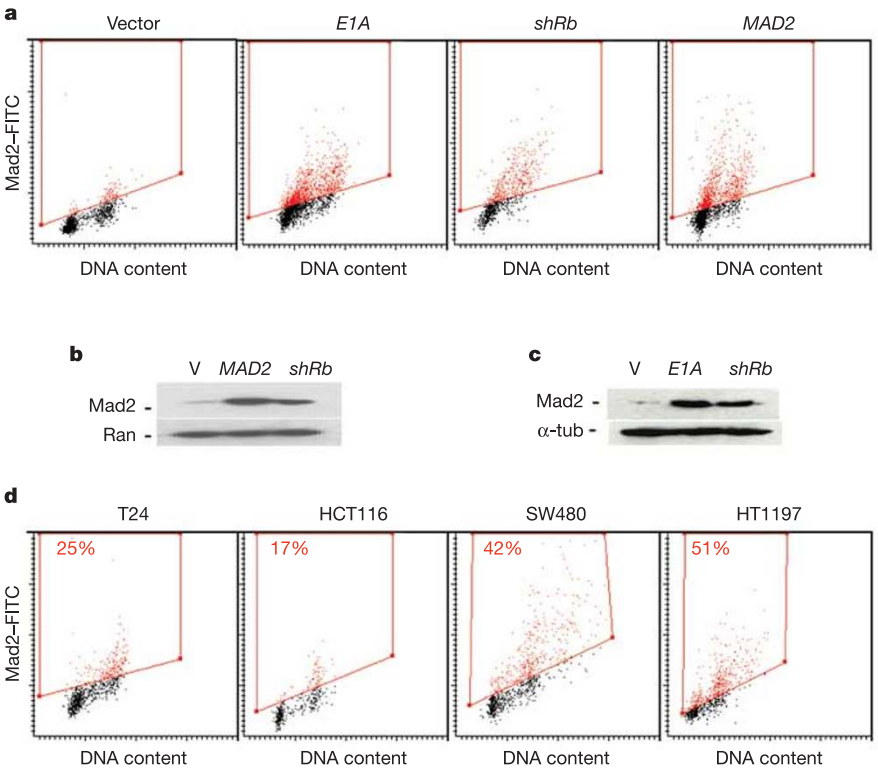

Figure 2 Deregulating the Rb/E2F pathway produces aberrant Mad2 expression. **a**, Biparametric analysis of Mad2 expression and DNA content by LSC in IMR90 fibroblasts expressing a vector control (Vector), *E1A*, *shRb* or *MAD2*. **b**, **c**, Western blot analysis of Mad2 in the cells described in part **a**. Ran and α-tubulin (α-tub) protein levels serve as loading controls. **d**, LSC analysis of Mad2 expression and DNA content in T24, HCT116, HT1197 and SW480 tumour derived lines. Numbers indicate the total percentage of Mad2 positive cells.

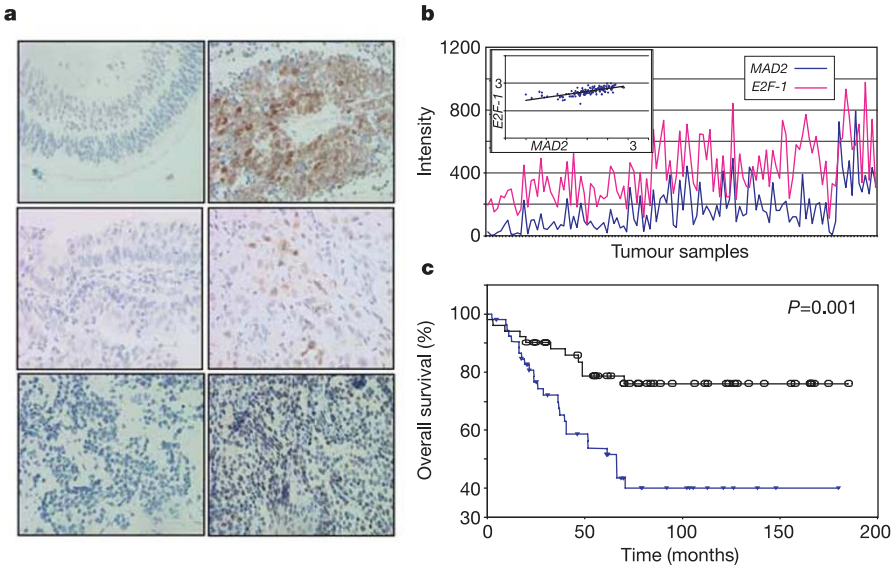

Figure 3 Abnormal Mad2 expression in human tumours. **a**, Immunohistochemistry for Mad2. Top: nearly undetectable Mad2 expression in normal retina (left) compared to high levels in retinoblastoma (right). Middle: an example of a Mad2-negative transitional cell carcinoma of the bladder (TCC, left) compared to a Mad2-positive invasive TCC (right). Bottom: a Mad2-negative (left) and positive (right) neuroblastoma. **b**, Comparison of *E2F-1* and *MAD2* transcript levels in a cohort of 106 neuroblastic tumours and 12 neuroblastoma cell lines[20]. The inset represents the logarithm of *MAD2* mRNA expression (X axis) versus *E2F-1* (Y axis), indicating a near-linear correlation. **c**, Kaplan–Meier survival curves stratified by *MAD2* microarray-based mRNA levels, with prognostic significance by the log-rank test using median values as cut points. Neuroblastoma cases with low (black curve) and high (blue curve) *MAD2* mRNA levels are shown.

NIH-3T3 cell populations accumulated cells with greater than 4c DNA content during the course of cell division (Fig. 4a). These effects were exacerbated by treatment with nocodozole, which acutely engages the spindle checkpoint (data not shown).

Analogous results were obtained using fluorescent *in situ* hybridization (FISH) to track specific chromosomes. The *E1A*-, *shRB*- and *MAD2*-expressing populations each accumulated cells with aberrant chromosome numbers (Fig. 4b, c). In contrast, IMR90 cells expressing a control vector retained normal chromosome content upon serial passaging (Fig. 4a–c, see Vector or V) and responded normally to nocodazole (data not shown). Chromosome counting of metaphase spreads confirmed that IMR90 and HCT116 cells with defective Rb or elevated Mad2 are frequently aneuploid (Fig. 4c). No centrosome amplification was detected in *E1A*- or *MAD2*-transduced fibroblasts by γ-tubulin (see Supplementary Fig. S3b) or β-tubulin immunofluorescence staining (spindle shape analysis; data not shown), suggesting that the observed mitotic defects are not due to the effects of cyclin E on centrosome duplication[24,25]. However, as cyclin E is an E2F target, centrosome amplification may exacerbate the chromosomal instability associated with Rb loss. Nevertheless, misexpression of Mad2 is sufficient to produce this phenotype.

We next examined mitotic progression of individual cells in *E1A*-, *shRb*-, *MAD2*- or vector-transduced populations co-expressing green fluorescent protein (GFP)-tagged histone (H2B–GFP), by phase contrast and fluorescence videomicroscopy. Whereas normal NIH-3T3 cells underwent an orderly and rapid mitosis, cells expressing E1A or shRb took an unusually long time to finish the process, displaying marked difficulties in completing cytokinesis (Fig. 5a–c; Supplementary Fig. S4a and S5, compare video A with C and D) and frequent defects in chromosome segregation (Fig. 5c; Supplementary Fig. S5, compare video B with G). Cells expressing Mad2 alone displayed similar defects (Fig. 5c; Supplementary Fig. S5, compare video A with E and F), although the chromosome segregation abnormalities were more pronounced, perhaps owing to the higher Mad2 levels that these populations expressed (Supplementary Fig. S5, compare video B with H). Similar phenotypes were also observed in *E1A*-, *shRb*- and *MAD2*-transduced HCT116 (Supplementary Fig. S5, videos I and J). In each cell population, the frequency of aberrant mitoses decayed after serial passaging, perhaps owing to lethality of cells with aberrant chromosome content and/or to cellular adaptation to elevated Mad2. Nevertheless, consistent with a prolonged mitosis, cells aberrantly expressing Mad2 displayed a delay in the degradation of securin and cyclin B (Supplementary Fig. S4b, c), whose sequential ubiquitination by the APC/cyclosome is inhibited by

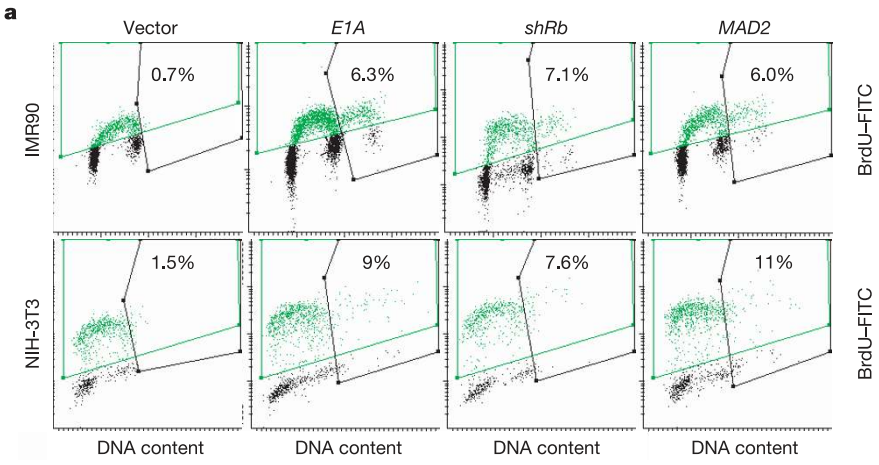

c

FISH (percentage aneuploid cells)							
IMR90					HCT116		
V	*E1A*	*E2F*	*shRB*	*MAD2*	V	*shRB*	*MAD2*
5	11	20	15	15	4	10	20

Karyotyping (percentage tetraploid cells)							
IMR90				HCT116			
V	*shRB*	*E1A*	*MAD2*	V	*shRB*	*E1A*	*MAD2*
0	5	7.5	10	3.3	11.2	13.3	30

Figure 4 Cells with defective Rb or elevated Mad2 display chromosomal instability. **a**, Immunocytochemical detection of BrdU versus DNA content by LSC in asynchronous cultures of IMR90 (upper panels) or NIH-3T3 (lower panels) infected with *E1A, shRB* or *MAD2*. **b**, FISH analysis on IMR90 cells, with centromeric probes for chromosomes 1 and 17 and DAPI counterstaining. **c**, Quantification of ploidy alterations derived from *E1A*, *shRb* or *MAD2* expression. FISH in IMR90 and HCT116 transduced cells (upper table). Shown are percentages of cells with abnormal number of positive signals for one or both probes. Percentage of infected cells exhibiting tetraploidy in metaphase spreads (lower table).

Mad2[7,13] and required for chromosome segregation and cytokinesis, respectively[6,7,26].

Complete downregulation of Mad2 in cells with intact Rb produces aneuploidy after a premature anaphase[27]. However, if Mad2 upregulation contributes to chromosome instability, we reasoned that a partial suppression of Mad2 in Rb defective cells would have the opposite effect—perhaps reducing the occurrence of aneuploid cells. Therefore, we used stable RNAi to partially suppress Mad2 in control, *E2F*- or *E1A*-transduced HCT116 cells. Consistent with a previous report[27], stable expression of two independent short-hairpin RNAs (*shMAD2*) in cells with low Mad2 levels further reduced Mad2 expression and increased the percentage of aneuploid cells (data not shown). In contrast, co-expression of *shMAD2* with *E2F* or *E1A* significantly reduced Mad2 to nearly normal levels (Fig. 5d, compare lanes 3 with 7 or 2 with 8) and reduced the fraction of aneuploid cells (Fig. 5e, f) without affecting E1A or E2F-1 levels (Supplementary Fig. S4d). Cells coexpressing *shMAD2* and either *E2F-1* or *E1A* were proliferating and showed similar S phase content compared to cells harbouring a control shRNA (data not shown). Therefore, although other Rb targets may contribute to chromosome instability, aberrant Mad2 activity is important for this process.

We suggest that aberrant expression of Mad2 arising as a result of Rb pathway defects can produce a hyperactive spindle checkpoint, thereby altering the sequence of mitotic events and the accuracy of chromosome transmission. Persistent inactivation of the APC/cyclosome, mediated by Mad2 signalling, delays the degradation of securin and cyclin B. Moreover, overexpression of securin (Pds1, PTTG)—observed in many different tumour types—produces aneuploidy and displays transforming activity *in vivo* and *in vitro*[28]. Interestingly, the behaviour of cells with aberrant Mad2 expression is reminiscent of cells treated for prolonged periods with nocodozole—following spindle checkpoint activation, these cells eventually adapt and enter the next cell cycle without a proper mitosis[29]. Together, our results demonstrate that deregulated Mad2 expression contributes to mitotic alterations and chromosome instability in the context of an altered Rb/E2F pathway.

Our data illustrate how aneuploidy in human cancers can arise as a byproduct of the Rb pathway defects that accompany tumorigenesis. During normal cell proliferation, the cell cycle is hardwired to

a

	Vector	*shRB*	*E1A*	*MAD2*
Number of divisions	*n*=23	*n*=38	*n*=11	*n*=22
Time (min)	75±3	114±12	114±15	113±7
P		*P*=0.0163*	*P*=0.0012***	*P*<0.0001***

b

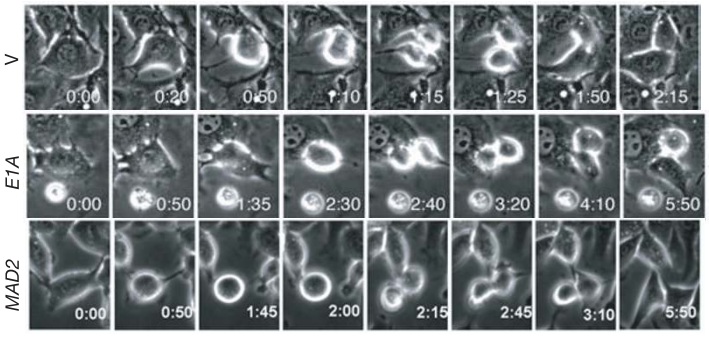

c

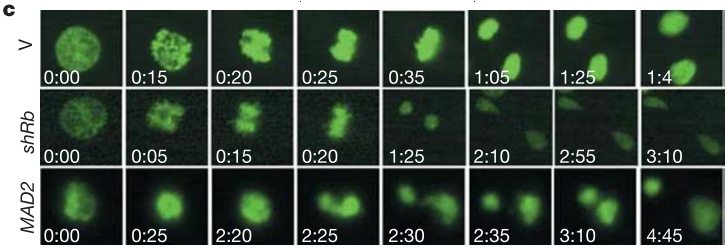

d

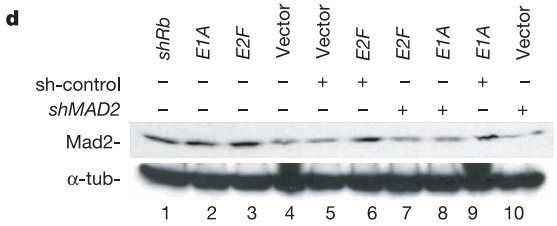

e

Karyotyping						
	E2F + shRNA control		*E2F* + *shMAD2A*		*E2F*+ *shMAD2B*	
DNA content	2c	4c	2c	4c	2c	4c
Percentage of cells	93	7	97	3	98	2

f

FISH																				
	Noc. *t* (h)	*E2F* + shRNA control				*E2F* + *shMAD2A*				*E2F* + *shMAD2B*				*E1A*				*E1A* + *shMAD2A*			
Number of signals		1	2	3	>3	1	2	3	>3	1	2	3	>3	1	2	3	>3	1	2	3	>3
Percentage of cells	0 h		85	10	5	1	95	4		2	95	3		5	91	3	1		98	1	1
	12 h		70	25	5		95	5			90	8	2								

Figure 5 Aberrant Mad2 expression contributes to the mitotic defects associated with Rb loss. **a**, Average time needed to complete mitosis in NIH-3T3 cells expressing control vector, *shRb*, *E1A* or *MAD2* assessed from prometaphase (disruption of the nuclear envelope and chromatin condensation) to completed cytokinesis and reattachment of daughter cells. *n*, number of cells analysed. *P* values determined by Student's *t*-test. **b**, Time course of a normal mitotic division occurring in vector-transduced NIH-3T3 cells (v). Illustrative examples of prolonged mitoses occurring in cells expressing *E1A*, *shRb* or *MAD2* (*E1A*- and *MAD2*-transduced NIH-3T3 cells shown). **c**, A fluorescence videomicroscopy series of H2B–GFP transfected cells showing normal chromosome segregation (vector-transduced NIH-3T3, v) and representative examples of the slow and abnormal chromosomal excision patterns observed in cells expressing *shRb*, *E1A* or *MAD2* (*shRb* and *MAD2* shown). **d**, Immunoblotting for Mad2 in HCT116 cells expressing *E2F*-, *E1A*- or Vector together with either a *MAD2* hairpin (*shMAD2*) or a hairpin control (sh-control) as indicated. **e**, **f**, Cytogenetic analyses by karyotyping (**e**) or FISH (**f**) of HCT116 cells co-expressing *E2F* or *E1A* with a *MAD2* shRNA (two sequence-independent hairpins, *shMAD2A* and *shMAD2B*) or a shRNA control. ≥200 interphase nuclei were analysed by FISH. Values were compared for statistical significance using the exact test of Fisher: $P = 0.015$ and $P < 0.0001$, comparing E2F-transduced cells coinfected with *shMAD2A* or shRNA control, at 0 and 12 h nocodazole (Noc.); $P = 0.006$ and $P = 0.0007$, for *shMAD2B* versus shRNA control, at 0 and 12 h respectively.

the spindle checkpoint through E2F, presumably to ensure that Mad2 expression is tightly controlled. As a consequence, mutations that disrupt Rb function produce deregulated E2F activity leading to inappropriate proliferation, but also aberrant Mad2 expression and, eventually, aneuploidy. Hence, our results provide one explanation for why loss-of-function mutations in spindle checkpoint genes are uncommon in human cancers[11,12]. Our model also implies that aneuploidy is not necessarily a selected trait of cancer cells but can be an inadvertent consequence of defects that uncouple mitotic control from normal cell cycle progression. Nevertheless, this byproduct of Rb loss might subsequently increase the mutation rate, thereby fuelling further tumour evolution. □

Methods

Cells, gene transfer and drug treatment

Human tumour cell lines (T24, HT1197, HCT116, SW480 and U-2OS), normal human fibroblasts (IMR90) and murine immortal fibroblasts (NIH-3T3) were obtained from the ATCC (American type culture collection, Rockville). Primary MEFs were isolated and cultured as described[15]. Cells were infected with high-titre recombinant retroviruses expressing *E1A* (LPC–12S), *E2F-1* (LPC–E2F1), *shRb* (MSCV–shRB)[16], *shMAD2* (MSCV–shMAD2A or B)[27], *shmurMAD2* (shRNA control, MSCV–shmurMAD2)[27] or *MAD2* cDNA (Babe–MAD2) and selected with puromycin ($2\,\mu g\,ml^{-1}$)[15]. Adenoviruses *E1A*, *E2F-1* and *GFP* control were used at a multiplicity of infection of 100 PFU $cell^{-1}$ as described[15]. Nocodazole (Sigma) was used at 200 nM and 400 nM for normal fibroblast or tumour cell lines, respectively.

Protein and mRNA expression

Protein expression was assessed by immunoblotting using 30 μg of total cell lysate[15]. Blots were probed with antibodies directed against hsMad2 (clone 48, BD Biosciences), E1A (M58, BD Biosciences), p53 (CM5, Novocastra), E2F-1 (KH95, Santa Cruz), Cyclin A (BF683, Santa Cruz), Ran (sc-1156, Santa Cruz), Pds1 (ab-1, DCS-280, Neomarkers), cyclin B1 (05-373, Upstate), phospho-histone3 (06-570, Upstate), APC2 (ab-1, Neomarkers) or α-tubulin (B-5-1-2, Sigma). Anti-mouse, anti-rabbit (Amersham) or anti-goat horseradish peroxidase (HRP) (Sigma) were used as secondary antibodies and proteins were visualized using an ECL detection system (Amersham). mRNA levels were assessed by northern blotting using 10 μg of total RNA[15].

LSC and FACS

Cells grown as monolayers on microscope-chamber slides were washed, fixed and incubated with the respective antibodies[30]: hsmad2 (BD Biosciences); alpha-tubulin FITC conjugated (clone DM 1A) and γ-tubulin (Sigma); and anti-Rb (Pharmingen, BD Laboratories). Mouse IgG served as an isotype negative control. Cells were washed and incubated with FITC-conjugated rabbit anti-mouse F(ab')2 or anti-rabbit (DAKO), then washed and incubated with $5\,\mu g\,ml^{-1}$ of propidium iodide (PI; Molecular Probes) and 0.1% RNase A (Sigma) in PBS before measurement by LSC (CompuCyte) as indicated[30]. A minimum of 3,000 cells were analysed per slide as previously described[30].

Cell cycle analysis after low-serum synchronization of IMR90 cells was performed as previously described[15]. Mitotic index was quantified by measuring MPM2 expression (anti-MPM2, Upstate Biotechnology) versus DNA content (PI) by FACS[27]. For BrdU incorporation assays, slide-grown cells were incubated in 10 μM BrdU (Sigma) for 1 h 30 min (human cell lines) or 3 h (normal fibroblasts) immediately before collection. Cells were fixed with 80% ethanol overnight and incubated with FITC-conjugated anti-BrdU antibody after denaturing the DNA, following the manufacturer's instructions (Pharmingen, BD Laboratories). BrdU incorporation was measured by LSC, with the equivalent FITC-conjugated isotypic control as a baseline.

Chromosome analyses

Bicolour FISH was performed using probes for chromosomes 1 and 17 centromere-specific alphoid region (Vysis)[20]. The number of hybridization signals for each probe was assessed in a minimum of 200 interphase nuclei with strong and well-delineated contours. Chromosome analysis of cells in metaphase was performed as described[27].

Immunohistochemistry

Sections were deparaffinized, treated with 1% H_2O_2, immersed in boiling 10 mM citrate buffer for 15 min and incubated in 10% normal horse serum for 30 min at room temperature. Anti-hsmad2 (Transduction Laboratories, BD Laboratories; dilution 1:100) and anti-human Ki-67 (MIB-1, DAKO; dilution 1:1000) antibodies were used. Samples were then incubated with biotinylated anti-mouse IgG at 1:500 dilution (Vector Laboratories) followed by avidin–biotin peroxidase complexes (1:25; Vector Laboratories) for 30 min. Diaminobenzidine was used as the chromogen, and hematoxylin as the nuclear counterstain.

Human tumour samples and gene expression analysis

Twelve cases of retinoblastoma and 95 bladder tumours on a tissue array were analysed by immunohistochemistry. In addition, 12 neuroblastoma cell lines and 106 neuroblastic tumours were studied[20]. Total RNA was extracted and cDNA was labelled and hybridized to Affymetrix human U95 oligonucleotide arrays as described[20]. Comparisons of *E2F-1*, *MAD2* and *MYCN* expression levels were performed by Kendall's *tau* correlation test. Kaplan–Meier survival curves were generated by using the SPSS program (SPSS). *E2F-1*, *MYCN* and *MAD2* expression were tested for prognostic significance ($P < 0.05$) by the log-rank test using median values as cut points. Protein expression was validated on a tissue microarray containing 50 neuroblastoma cases.

Received 15 April; accepted 6 July 2004; doi:10.1038/nature02820.

1. Hanahan, D. & Weinberg, R. A. The hallmarks of cancer. *Cell* **100,** 57–70 (2000).
2. Albertson, D. G., Collins, C., McCormick, F. & Gray, J. W. Chromosome aberrations in solid tumors. *Nature Genet.* **34,** 369–376 (2003).
3. Dyson, N. The regulation of E2F by pRB-family proteins. *Genes Dev.* **12,** 2245–2262 (1998).
4. Jallepalli, P. V. & Lengauer, C. Chromosome segregation and cancer: cutting through the mystery. *Nature Rev. Cancer* **1,** 109–117 (2001).
5. Cahill, D. P. *et al.* Mutations of mitotic checkpoint genes in human cancers. *Nature* **392,** 300–303 (1998).
6. Cleveland, D. W., Mao, Y. & Sullivan, K. F. Centromeres and kinetochores: from epigenetics to mitotic checkpoint signaling. *Cell* **112,** 407–421 (2003).
7. Yu, H. Regulation of APC-Cdc20 by the spindle checkpoint. *Curr. Opin. Cell Biol.* **14,** 706–714 (2002).
8. Kalitsis, P., Earle, E., Fowler, K. J. & Choo, K. H. *Bub3* gene disruption in mice reveals essential mitotic spindle checkpoint function during early embryogenesis. *Genes Dev.* **14,** 2277–2282 (2000).
9. Dobles, M., Liberal, V., Scott, M. L., Benezra, R. & Sorger, P. K. Chromosome missegregation and apoptosis in mice lacking the mitotic checkpoint protein Mad2. *Cell* **101,** 635–645 (2000).
10. Michel, L. S. *et al.* MAD2 haplo-insufficiency causes premature anaphase and chromosome instability in mammalian cells. *Nature* **409,** 355–359 (2001).
11. Cahill, D. P. *et al.* Characterization of MAD2B and other mitotic spindle checkpoint genes. *Genomics* **58,** 181–187 (1999).
12. Hernando, E. *et al.* Molecular analyses of the mitotic checkpoint components *hsMAD2*, *hBUB1* and *hBUB3* in human cancer. *Int. J. Cancer* **95,** 223–227 (2001).
13. Wassmann, K. & Benezra, R. Mad2 transiently associates with an APC/p55Cdc complex during mitosis. *Proc. Natl Acad. Sci. USA* **95,** 11193–11198 (1998).
14. Ren, B. *et al.* E2F integrates cell cycle progression with DNA repair, replication, and G(2)/M checkpoints. *Genes Dev.* **16,** 245–256 (2002).
15. Nahlé, Z. *et al.* Direct coupling of the cell cycle and cell death machinery by E2F. *Nature Cell Biol.* **4,** 859–864 (2002).
16. Narita, M. *et al.* Rb-mediated heterochromatin formation and silencing of E2F target genes during cellular senescence. *Cell* **113,** 703–716 (2003).
17. Sanchez-Carbayo, M. *et al.* Molecular profiling of bladder cancer using cDNA microarrays: defining histogenesis and biological phenotypes. *Cancer Res.* **62,** 6973–6980 (2002).
18. Arber, N. *et al.* Antisense to cyclin D1 inhibits the growth and tumorigenicity of human colon cancer cells. *Cancer Res.* **57,** 1569–1574 (1997).
19. Dalbagni, G., Presti, J., Reuter, V., Fair, W. R. & Cordon-Cardo, C. Genetic alterations in bladder cancer. *Lancet* **324,** 469–471 (1993).
20. Alaminos, M. *et al.* Genome-wide analysis of gene expression associated with *MYCN* in human neuroblastoma. *Cancer Res.* **63,** 4538–4546 (2003).
21. Schuldiner, O. & Benvenisty, N. A DNA microarray screen for genes involved in c-MYC and N-MYC oncogenesis in human tumors. *Oncogene* **20,** 4984–4994 (2001).
22. Van 't Veer, L. J. *et al.* Gene expression profiling predicts clinical outcome of breast cancer. *Nature* **415,** 530–536 (2002).
23. Lentini, L., Pipitone, L. & Di Leonardo, D. Functional inactivation of pRB results in aneuploid mammalian cells after release from a mitotic block. *Neoplasia* **4,** 380–387 (2002).
24. Spruck, C. H., Won, K. A. & Reed, S. I. Deregulated cyclin E induces chromosome instability. *Nature* **401,** 297–300 (1999).
25. Okuda, M. *et al.* Nucleophosmin/B23 is a target of CDK2/cyclin E in centrosome duplication. *Cell* **103,** 127–140 (2000).
26. Stemmann, O., Zou, H., Gerber, S. A., Gygi, S. P. & Kirschner, M. W. Dual inhibition of sister chromatid separation at metaphase. *Cell* **107,** 715–726 (2001).
27. Michel, L. *et al.* Complete loss of the tumor suppressor MAD2 causes premature cyclin B degradation and mitotic failure in human somatic cells. *Proc. Natl Acad. Sci. USA* **101,** 4459–4464 (2004).
28. Zou, H., McGarry, T. J., Bernal, T. & Kirschner, M. W. Identification of a vertebrate sister-chromatid separation inhibitor involved in transformation and tumorigenesis. *Science* **285,** 418–422 (1999).
29. Lanni, J. S. & Jacks, T. Characterization of the p53-dependent postmitotic checkpoint following spindle disruption. *Mol. Cell. Biol.* **18,** 1055–1064 (1998).
30. Darzynkiewicz, Z., Gong, J., Juan, G., Ardelt, B. & Traganos, F. Cytometry of cyclin proteins. *Cytometry* **25,** 1–13 (1996).

Supplementary Information accompanies the paper on **www.nature.com/nature**.

Acknowledgements We thank M. Narita for providing the shRb construct, M. Lu for the bladder tissue microarray, S. Menendez for technical assistance and A. Kel for the use of the SiteScan program. We thank the Molecular Cytology and the Flow Cytometry Core Laboratories at Memorial Sloan-Kettering and P. McCloskey from CSHL flow cytometry facility for technical assistance. Also, we thank S. Gangadharan, R. Dickins, S. Gonzalez, N. Abumrad, B. Stillman and P. P. Pandolfi for reading the manuscript. We also thank all the members of the Lowe and Cordon-Cardo laboratories for discussions. This work was supported by program project grants from the NCI (S.W.L. and C.C.C.), Clinical Investigator Research Development Awards (L.M. and R.B.), DOD-Breast Cancer Research Program fellowship award (Z.N.), a Fundacion Caja Madrid-CNIO-MSKCC fellowship (E.H. and M.A.), a Fellowship from the Spanish Ministry of Education, Culture and Sports (E.D.R.), a US NCI postdoctoral training grant (M.T.H.) and gifts from the Laurie Strauss Leukemia Foundation and the Herbert J. Siegel philanthropic fund.

Competing interests statement The authors declare that they have no competing financial interests.

Correspondence and requests for materials should be addressed to S.W.L. (lowe@cshl.edu).